ACS Catalysis

Research Article

Cite This: ACS Catal. 2018, 8, 9034−9042

pubs.acs.org/acscatalysis

Quantifying Confidence in DFT Predicted Surface Pourbaix Diagrams and Associated Reaction Pathways for Chlorine Evolution

Vaidish Sumaria,[†,‡] Dilip Krishnamurthy,[‡] and Venkatasubramanian Viswanathan*[,†,‡]

[†]Department of Chemical Engineering, Carnegie Mellon University, Pittsburgh, Pennsylvania 15213, United States

[‡]Department of Mechanical Engineering, Carnegie Mellon University, Pittsburgh, Pennsylvania 15213, United States

Supporting Information

ABSTRACT: Catalytic activity predictions and the identification of active sites rely on precisely determining the dominant reaction mechanism. The activity governing mechanism and products could vary with the catalyst material, which can be described by material descriptor(s), typically the binding strength(s) of key intermediate species. Density functional theory calculations can be used to identify dominant reaction mechanisms. However, the dominant reaction mechanism is sensitive to the choice of the exchange-correlation functional. Here, we demonstrate this using the chlorine evolution reaction on rutile oxides as an example, which can occur through at least three reaction mechanisms each mediated by different surface intermediates and active sites. We utilize Bayesian error estimation capabilities within the BEEF-vdW exchange-correlation (XC) functional to quantify the uncertainty associated with predictions of the operative reaction mechanism by systematically propagating the uncertainty originating from DFT-computed adsorption free energies. We construct surface Pourbaix diagrams based on the calculated adsorption free energies for rutile oxides of Ru, Ir, Ti, Pt, V, Sn, and Rh. We utilize confidence value (c value) to determine the degree of confidence in the predicted surface phase diagrams. Using the scaling relations between the adsorption energies of intermediates, we construct a generalized Pourbaix diagram showing the stable surface composition as a function of potential and the oxygen binding energy on the cus site (ΔE_{O^c}). This allows us to incorporate consistency between activity and surface stability, which is necessary to determine activity volcano relationships for surface reactivity. We incorporate the uncertainty in linear scaling relations to quantify the confidence in generalized Pourbaix diagram and the associated activity. This allows us to compute the expectation limiting potential as a function of ΔE_{O^c}, which provides a more appropriate activity measure incorporating DFT uncertainty. We show that the confidence in the classification problem of identifying the active reaction mechanism is much higher than that for the prediction problem of determining catalytic activity. We believe that such a systematic approach is needed for accurate determination of activities and reaction pathways for multielectron electrochemical reactions such as N_2 and CO_2 reduction.

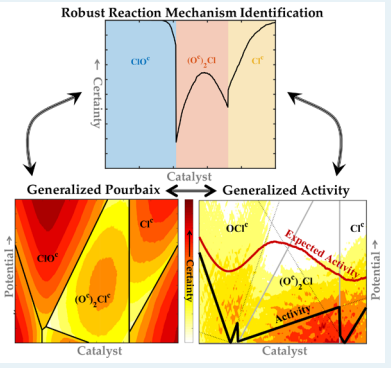

KEYWORDS: *reaction mechanism, Pourbaix diagrams, uncertainty propagation, chlorine evolution, catalytic activity*

1. INTRODUCTION

A major challenge in surface electrocatalysis involves identifying the dominant reaction mechanism from the many possible competing electrochemical reactions at the electrode/electrolyte interface.[1] This is further complicated by the dynamic state of the surface depending on the external conditions: e.g., electrode potential, pH, and aqueous electrolyte.[2−5] The coupling between surface state and dominant reaction mechanism is crucial for important electrochemical reactions like chlorine evolution,[5] hydrogen evolution,[6] nitrogen reduction,[7] and carbon dioxide reduction.[8−14]

Experimentally, macrokinetic measurements, to determine reaction orders, pH dependence, and Tafel slope, can provide useful insights but typically several competing mechanistic pathways could still provide a plausible explanation for all the data.[5,15] An emerging frontier is using spectroscopic methods to identify stable surface species, e.g., infrared spectroscopy and ambient pressure XPS in conjunction with electrochemical measurements, to identify the dominant mechanistic pathways.[12,16−19]

First-principles calculations have been used to identify probable reaction mechanisms through a combination of surface Pourbaix diagrams and free energy diagrams for the different mechanistic pathways.[5,20] However, it is well-known that DFT calculations have finite accuracy; hence, a key question that emerges is the likelihood of the identified dominant reaction pathways. Systematic progress in quantifying uncertainty within DFT has been made with the incorporation of Bayesian error estimation capabilities[21] into exchange-correlation functionals. This has been used to quantify the uncertainty associated with reaction rates in heterogeneous catalysis[22] and electrocatalysis.[23] More recently, we showed that uncertainty quantification can be used as a tool to decide the most appropriate descriptor for

Received: April 11, 2018
Revised: July 13, 2018
Published: August 13, 2018

DOI: 10.1021/acscatal.8b01432
ACS Catal. 2018, 8, 9034−9042

computational predictions.[24] However, these analyses make simplistic assumptions about the state of the surface and do not incorporate a self-consistent loop between activity and surface stability, necessary to determine surface reactivity.

In this work, we demonstrate an approach to accurately incorporate a self-consistent loop between surface state and reaction pathways while systematically incorporating uncertainty associated with chemisorption energies. We apply this approach to an important electrochemical reaction, chlorine evolution. This reaction is chosen for its industrial importance[25] and the complexities involved in mapping the selectivity with respect to oxygen evolution reaction.[26] Prior work by Hansen et al.[5] showed that the overpotential for oxygen evolution to occur on rutile oxides, which involves three oxygen intermediates, is always higher than that for chlorine evolution.[27] This can be rationalized on the basis of the fact that finding a catalyst material for an electrochemical reaction involving more elementary steps is generally challenging owing to inherent scaling relations.[28] Hence, we focus on the reaction mechanisms for the chlorine evolution reaction on rutile oxides. In this analysis, we begin with constructing the Pourbaix diagram for rutile oxides of Ru, Ir, Ti, Pt, V, Sn, and Rh. Inspired by the work of Hansen et al.,[5] we determine a generalized Pourbaix diagram with the activity volcano relationships of the multiple reaction mechanisms to develop a generalized trimodal activity relationship. We use a previously defined quantity, c value, to quantify confidence in surface phase diagrams. Through the error-estimation approach, an ensemble of generalized Pourbaix diagrams are constructed that lead to an ensemble of generalized activity relationships. We compute the expected activity for a range of material descriptor values, which is the probability-weighted average of the predicted limiting potentials. Finally, we utilize this approach to determine the likelihood of reaction mechanisms for different material descriptor values. We quantify this through a variant of the c value metric to determine the reaction mechanism prediction confidence. An important conclusion is that confidence associated with reaction mechanisms is much greater than the predicted activity values. We believe this will be crucial to accurately understand different reaction mechanisms and thereby the activity and the nature of the active site.

2. METHODS

2.1. Calculation Details. Calculations were performed using the projector augmented-wave (PAW) method[29] as implemented in the GPAW package[30] using the Bayesian error estimation functional with van der Waals correlation (BEEF-vdW), which has built-in error estimation capabilities. This functional is developed on the basis of Bayesian statistics, which defines the probability distribution (P) for the model parameters (a) given a model (θ) and training data set (D) as $P(a|\theta, D) \approx \exp[-C(a)/\tau]$. Here, $C(a)$ is the cost function consisting of a squared error term and a regularization term to avoid overfitting and τ is a cost "temperature". Given a data set D (comprising of several experimental sets of energetic and structural data describing bonding in chemical and condensed matter systems), the model perturbation δa is associated with a certain probability that defines an ensemble of exchange correlation functionals.[31] The electron density of a self-consistent DFT calculation converged using the best-fit model parameters is used along with the distribution of fitting parameters to non-self-consistently generate an ensemble of energies which is representative of the error in the predictions of the best-fit functional with respect to the experimental training data.[22,23,31−33] The cost temperature (τ) is chosen with no rescaling,[22] consistent with prior work,[23,24,32,33] such that generated ensemble energies reproduce the known experimental errors in the entire benchmark data set.

A periodically repeated slab with 12 atomic layers (4 O−M−O repeat units; M = metal) is chosen for all the considered rutile oxide (110) surfaces of RuO_2, IrO_2, TiO_2, PtO_2, RhO_2, SnO_2, and VO_2.[27] A schematic of the surface used in this work is shown in Figure S1 in the Supporting Information. A 4 × 4 × 1 Monkhorst−Pack type k-point grid was used for a 2 × 1 surface unit cell with two bridge and two cus (superscript b and c, respectively) sites. The two bottom layers of the unit cell were kept fixed, and the top two layers with the adsorbates were allowed to relax with a force criterion of <0.05 eV/Å. A Fermi smearing of 0.01 eV was used, and all calculated energies were extrapolated to an electronic temperature of 0 K.

Following the work of Hansen et al.,[5] we considered adsorption of the intermediates OH^b and O^b at the bridge site and adsorption of O^c, HO^c, Cl^c, HOO^c, and ClO^c at the coordinatively unsaturated site (cus) and the adsorption of O_2^{cc} and $Cl(O^c)_2$ at adjacent cus sites. All relevant combinations involving the two adsorption sites and the various adsorbates were considered. For the range of reaction conditions relevant to chlorine evolution, the bridge sites bind intermediates relatively strongly and are thereby covered with oxygen. The adsorption energies of the considered adsorbates are referenced to chlorine and hydrogen gas.[5] We use gas-phase H_2O as the reference state for oxygen, by assuming chemical equilibrium with liquid water at 298 K and 0.035 bar,[34] to avoid the well-known errors made by DFT in describing O_2. Additionally, the effect of electric field in the Helmholtz layer is not taken into account, since its effect is negligible for adsorbates with small dipole moments perpendicular to the surface.[35]

The effect of solvation based on the foundational understanding developed on the interaction of water on metal surfaces has led to improved activity predictions.[36−40] The effect of the interaction of water and the solvation structure of water and oxygen intermediates are not established for the case of rutile oxides. A synergistic theoretical and experiment effort involving both ab initio molecular dynamics and X-ray spectroscopy is necessary to develop an understanding of the interaction between rutile oxides and water hydroxyl layers.[41] Therefore, in this work, the effect of solvation is assumed to be negligible on the considered oxide surfaces owing to the hydrophobicity of oxide surfaces, due to which a well-connected water network is typically not in registry with the underlying catalyst surface.[42,43]

2.2. Quantifying Confidence in Predicted Surface States. Pourbaix diagrams represent the landscape of the most thermodynamically stable state (minimum Gibbs free energy of adsorption) of a given surface over a range of operating potentials (U) and pH values. The ensemble of functionals results in an ensemble of Pourbaix diagrams, allowing us to obtain a measure of the confidence in a predicted surface state by quantifying the agreement between functionals. More precisely, we use the confidence value[33] (c value), which in this context can be defined as the fraction of the ensemble that is in agreement with the hypothesis of the best-fit (or optimal BEEF-vdW) functional, and is given by

DOI: 10.1021/acscatal.8b01432
ACS Catal. 2018, 8, 9034−9042

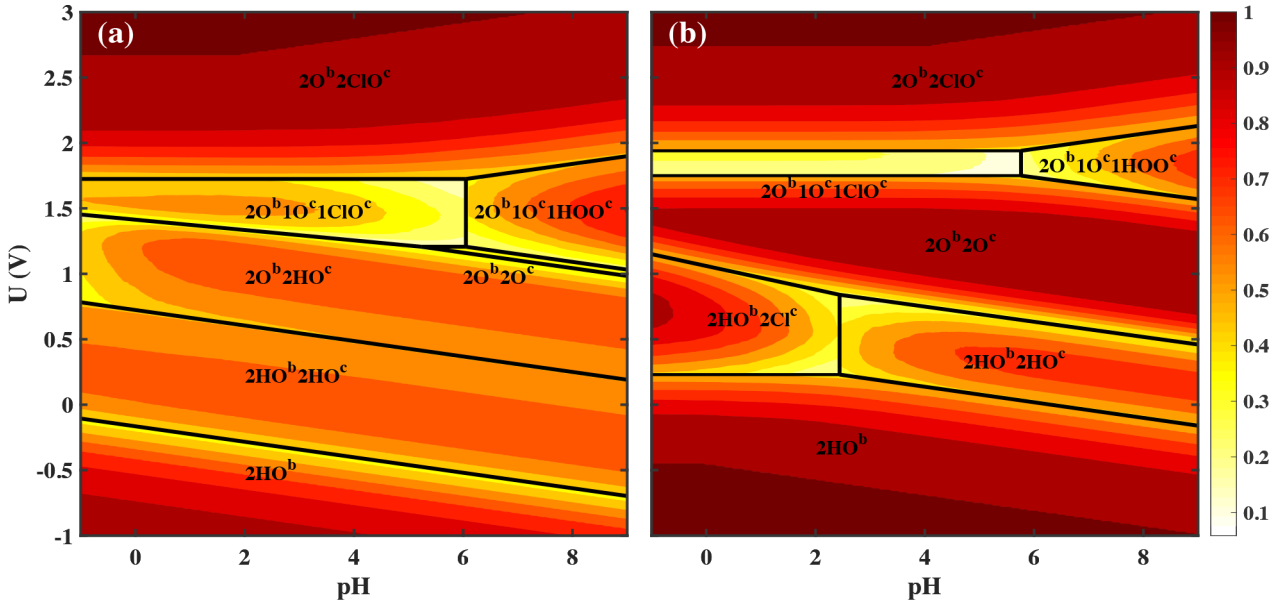

Figure 1. Surface Pourbaix diagrams for (a) IrO_2 and (b) RuO_2. The bridge and cus sites of adsorption on rutile (110) oxides have been denoted by the superscripts b and c, respectively. The black lines define the surface phase boundaries, and the stable surface states are depicted using the surface intermediate species. The two Pourbaix diagrams have been constructed for the catalyst surface in equilibrium with Cl^-, H^+, and H_2O at 298.15 K and $a_{Cl^-} = 1$. For both IrO_2 and RuO_2, we observe that chlorine evolution is mediated using the reaction mechanism involving the stable intermediate ClO^c. The uncertainty in the surface phase predictions has been quantified using the c value, which we define as a metric for prediction confidence in the context of Pourbaix diagrams. The c values of the associated predictions have been shown using a color map. Phase boundaries are characteristic of regions with low c values, identifying electrochemical operating regimes where DFT predictions are subject to higher uncertainty. Surface Pourbaix diagrams with associated c values for PtO_2, TiO_2, RhO_2, and SnO_2 are included in Figure S4 of the Supporting Information.

$$c(U, \mathrm{pH}) = \frac{1}{N_{\mathrm{ens}}} \sum_{n=1}^{N_{\mathrm{ens}}} \prod_{s_i \neq s_{\mathrm{opt}}} \Theta(\Delta G_{s_i}^n(U, \mathrm{pH}) - \Delta G_{s_{\mathrm{opt}}}^n(U, \mathrm{pH})) \quad (1)$$

where, $s_i \in S$, the set of all considered surface states, N_{ens} is the total number of functionals in the ensemble, and s_{opt} is the thermodynamically stable surface state predicted by the BEEF-vdW optimal functional at a given U and pH. $\Delta G_{s_i}^n$ refers to the adsorption free energy of the ith surface state given by the nth member of the ensemble of functionals. $\Theta(x)$ denotes the Heaviside step function.

2.3. Reaction Mechanisms and Expected Activity. We define the activity in terms of the limiting potential (U_L), given by the lowest potential at which all the involved reaction steps are downhill in free energy. The thermodynamic analysis forms a necessary criterion but could be insufficient, as we do not incorporate activation energies in the study due to the associated computational challenges in calculating them. It has been shown that this analysis remains consistent with a wide range of experiments on metals and alloys for oxygen reduction even when kinetics is taken into account.[44] Further, this framework has been used to rationalize trends in reactivity for oxygen reduction,[45] oxygen evolution,[27] and hydrogen evolution.[46]

The activity of rutile oxides is a function of the reaction pathway by which chlorine evolution could occur. We consider all the possible reaction mechanisms based on the thermodynamically stable chlorine containing reaction intermediates.

(I) Pathway mediated by the intermediate ClO^c:

$$O^c + Cl^-(aq) \rightarrow ClO^c + e^-$$

$$ClO^c + e^- + Cl^-(aq) \rightarrow O^c + Cl_2(g) + 2e^-$$

The limiting potential for this mechanism can be given as

$$U_L = U^{eq} + |\Delta G(ClO^c) - \Delta G(O^c)|/e$$

(II) Pathway mediated by the intermediate $Cl(O^c)_2$:

$$O_2^{cc} + Cl^-(aq) \rightarrow Cl(O^c)_2 + e^-$$

$$Cl(O^c)_2 + e^- + Cl^-(aq) \rightarrow O_2^{cc} + Cl_2(g) + 2e^-$$

The limiting potential for this mechanism can be given as

$$U_L = U^{eq} + |\Delta G(Cl(O^c)_2) - \Delta G(O_2^{cc})|/e$$

(III) Pathway mediated by the intermediate Cl^c:

$$Cl^-(aq) + c \rightarrow Cl^c + e^-$$

$$Cl^c + e^- + Cl^-(aq) \rightarrow c + Cl_2(g) + 2e^-$$

The limiting potential for this mechanism can be given as

$$U_L = U^{eq} + |\Delta G(Cl^c)|/e$$

We compute the expected limiting potential, $U_{EL}(\Delta E_{O^c})$, which is determined as the probability-weighted average of the limiting potential distribution, given by

$$U_{EL} = E[U_L] = \int_{U_L^{min}}^{U_L^{max}} U_L\, p(U_L)\, dU_L \quad (2)$$

where $p(U_L)$ is normalized such that $\int_{U_{min}}^{U_{max}} p(U_L)\, dU_L = 1$.[24] This approach relies on computing the probability distribution (Figure 4) of the predicted limiting potentials for chlorine evolution using the ensemble of the predicted activity volcanoes and the associated generalized phase diagrams (refer to section 3.3).

2.4. Quantifying Confidence in the Predicted Reaction Mechanism. The predicted active reaction mechanism for

DOI: 10.1021/acscatal.8b01432
ACS Catal. 2018, 8, 9034−9042

chlorine evolution varies with materials as a function of the chosen material descriptor, represented as $m_{pred}(\Delta E_{O^c})$, which maps any given value of ΔE_{O^c} to the corresponding reaction mechanism prediction from the set of possible mechanisms denoted by {0, 1, 2, ..., *i*, ..., *n*}, where *i* denotes the *i*th mechanism and $i = 0$ indicates no active mechanism. For chlorine evolution on rutile oxides, $n = 3$, as there are three distinct reaction mechanisms involved (refer to section 2.3). For materials where the reaction mechanism is mediated through ClO^c, we assign $m_{pred} = 1$. Similarly, when the mechanism is mediated through $Cl(O^c)_2$ and Cl^c, we assign $m_{pred} = 2$ and $m_{pred} = 3$, respectively.

We quantify the confidence in the predicted reaction mechanism as a function of ΔE_{O^c} through a Bayesian error-estimation approach similar to that outlined in section 2.2 for computing the confidence in predicted surface states. At each value of ΔE_{O^c}, the mechanism prediction confidence $c_{m_{pred}}(\Delta E_{O^c})$ is calculated as the fraction of the ensemble of functionals that is consistent with the predicted active mechanism based on the best-fit functional, $m^{opt}_{pred}(\Delta E_{O^c})$.

$$c_{m_{pred}}(\Delta E_{O^c}) = \frac{1}{N_{ens}} \sum_{n=1}^{N_{ens}} \delta(m^n_{pred}(\Delta E_{O^c}) - m^{opt}_{pred}(\Delta E_{O^c})) \quad (3)$$

where *n* denotes the *n*th functional, N_{ens} is the total number of functionals in the ensemble, and $\delta(x)$ denotes the Dirac delta function.

In regimes where the $c_{m_{pred}}$ value is lower than 1, it becomes important to determine whether the reaction mechanism predicted by the majority of functionals agrees with the optimal functional. This can be extended to determine a measure of confidence in any given reaction mechanism or the *i*th reaction mechanism m_i being operative. For example, for the mechanism mediated by ClO^c, $c_{m_{pred}=1}(\Delta E_{O^c})$, determines the fraction of functionals that predict that this mechanism is active. A generalized relation can be given as

$$c_{m_{pred}=i}(\Delta E_{O^c}) = \frac{1}{N_{ens}} \sum_{n=1}^{N_{ens}} \delta(m^n_{pred}(\Delta E_{O^c}) - i) \quad (4)$$

3. RESULTS AND DISCUSSION

3.1. Confidence in Stable Surface Phase Predictions. In this section, we attempt to answer the important question of the level of confidence in the predicted stable surface states for the active rutile oxides, using the approach outlined in section 2.2. Figure 1a depicts the surface phase diagram for IrO_2 with the associated *c* values indicating the likelihood of occurrence of the predicted surface Pourbaix diagram. Although there exist some differences in the positions of phase boundaries, we observe that the predicted set of stable surface states is consistent with that reported by Hansen et al.[5] The quantification of confidence in the predicted Pourbaix diagram allows us to identify regimes of high confidence as well as those with high uncertainty. We notice that regions predicted with low *c* values are close to surface phase boundaries. This identifies electrochemical operating regimes over which activity predictions based on the associated stable phase are subject to high uncertainty and require higher fidelity computations in conjunction with experimental validation.

A highly active catalyst for chlorine evolution entails $\Delta G \approx 0$ eV near $U = 1.36$ V for the formation of Cl^c. On IrO_2, we find that an active mechanism involving Cl adsorbed directly on an Ir cation is not operative for chlorine evolution. However, we observe that for a large range of pH ($0 \lesssim pH \lesssim 6$) ClO^c on the surface is thermodynamically stable for $U > 1.5$ V. This suggests that chlorine evolution on IrO_2 could be mediated by reaction pathway I, as described in section 2.3, consistent with the predictions using the RPBE XC.[5]

On RuO_2 (Figure 1b), we find that the predicted stable surface phases in this work compare well with those reported by Hansen et al. at low potentials ($U \lesssim 1$ V).[5] In this range of potentials, we observe a transition from only bridge sites being covered with OH to the surface being completely covered by OH with increasing *U*. At higher potentials ($\sim 1 \lesssim U \lesssim 1.8$ V), we find that the intermediates OH^b and OH^c both oxidize to O. A key difference that we find in our analysis relative to that reported by Hansen et al. is that oxygen association at the cus sites ($2O^c \rightarrow O_2^{cc}$) is endothermic by 0.82 eV. This implies that $2O^c$ is thermodynamically favorable relative to O_2^{cc}, which gets cascaded to the relative stability at higher potentials where we find that (i) $1O^c\ 1OOH^c$ is more stable than $1HO^c\ 1O_2^{cc}$ and (ii) $1O^c\ 1ClO^c$ is more stable than $Cl(O^c)_2$. This observation is comparable to the GGA-level DFT studies of Exner et al.[47] and Wang et al.,[48] who also predict that the O_2^{cc} adsorbate on RuO_2 should dissociate into $2O^c$. We also observe that oxygen is the most stable adsorbate with $U \approx 1.36$ V; Cl does not adsorb directly on the cus site for chlorine evolution to occur through reaction pathway I. Therefore, we conclude from the phase diagram that chlorine evolution on RuO_2 could be mediated by reaction pathway I. It is worth highlighting that using error estimation capabilities we quantify the confidence in the prediction that the oxygen association at the cus site is endothermic, which is the origin of the differences we observe relative to Hansen et al. We find that greater than 99.9% of the ensemble is in agreement with the prediction that oxygen association at the cus site is endothermic (refer to Figure S3 of the Supporting Information). This strengthens the need for the *c* value as a tool to quantify uncertainty in predictions of stable surface phases. The Pourbaix diagrams for the other rutile oxides are presented in the section 5 of the Supporting Information.

3.2. Scaling Relations and Generalized Surface Pourbaix Diagram. The stable state of the surface *S* is a function of pH, *U*, and the catalyst material M_{cat}. Pourbaix diagrams represent the stable surface state, *S*(pH,*U*), on a specific material. However, to analyze trends in the predicted stable surface states across materials, a generalized Pourbaix diagram that represents $S(U,M_{cat})$ for a fixed pH is required. This provides a computationally inexpensive way to understand the state of the catalyst surface without explicitly constructing Pourbaix diagrams for each material.

Generalized Pourbaix diagrams are constructed using a material descriptor to characterize the material M_{cat}, which is often chosen to be the adsorption energy of an intermediate. Hence, by invoking correlations (scaling relationships) between the adsorption energetics of various intermediates,[5] we construct a single descriptor model to predict stable surface state across materials. The adsorption energies of various intermediates (Cl, OH, ClO, O_2Cl, and O_2) at the cus site of the chosen oxides follow a linear relationship when they are plotted against the adsorption energy of oxygen at the cus site (using the BEEF-vdW optimal functional), as shown in Figure 2. This suggests that oxygen adsorption energy can be the continuous material descriptor choice for the reactivity of oxides.[5,49] ΔE_{O^c} is chosen as the material descriptor, since it allows a greater

DOI: 10.1021/acscatal.8b01432
ACS Catal. 2018, 8, 9034−9042

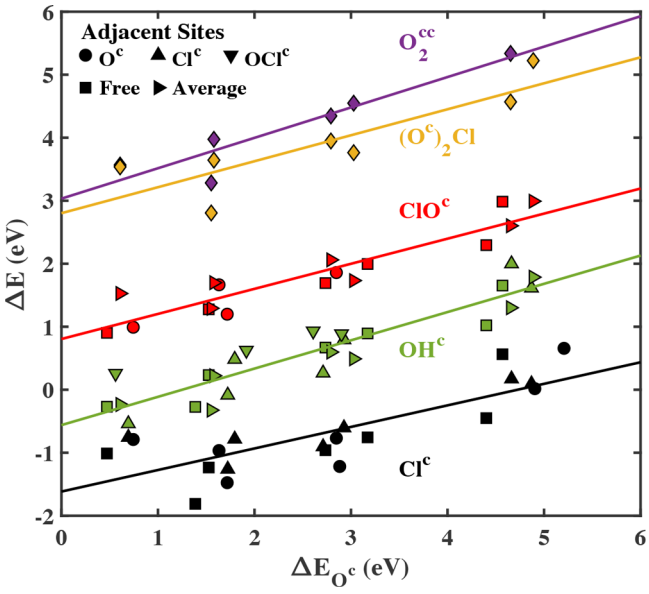

Figure 2. Adsorption free energies of various intermediates plotted against the adsorption free energy of oxygen on the cus site of rutile oxides to show the scaling relations between various intermediates. The figure represents the adsorption energy of Cl (black) at the cus site: $\Delta E_{Cl^c} = 0.34\Delta E_{O^c} - 1.62$ eV; adsorption energy of OH (green) at the cus site $\Delta E_{HO^c} = 0.45\Delta E_{O^c} - 0.56$ eV; adsorption energy of ClO (red) at the cus site $\Delta E_{ClO^c} = 0.4\Delta E_{O^c} + 0.81$; adsorption energy of $(O^c)_2Cl$ (yellow) at the cus site $\Delta E_{Cl(O^c)_2} = 0.41\Delta E_{O^c} + 2.8$ eV; adsorption energy of O_2^{cc} (purple) at the cus site $\Delta E_{O_2^{cc}} = 0.48\Delta E_{O^c} + 3.03$ eV. The symbols represent the nature of the site neighboring the adsorption site: (■) vacant neighboring cus site; (●) O^c neighbor; (▲) Cl^c neighbor; (▼) ClO^c neighbor. The symbol ▶ represents the average adsorption energy of the intermediate species for the fully covered surface, and ♦ represents the adsorption of energy of $(O^c)_2Cl$ (yellow) and O_2^{cc} (purple) plotted against the average adsorption energy of O for the fully covered surface. The fits here describe the scaling relations corresponding to the BEEF-vdW best-fit functional. The uncertainty in these fits is propagated through the outlined framework to quantify the confidence in the predicted generalized Pourbaix diagram (refer to Figure S5 in the Supporting Information).

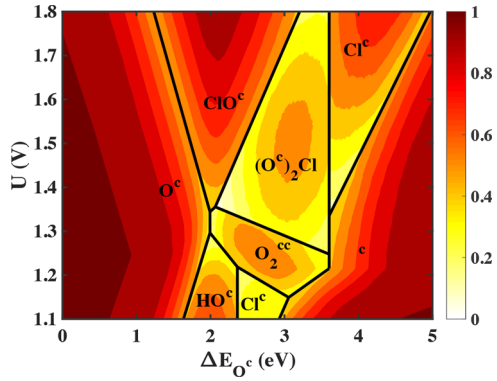

Figure 3. Generalized Pourbaix diagram showing the most stable surface at pH 0 and $a_{Cl^-} = 1$ as a function of potential and ΔE_O^c, the material descriptor. The black lines represent the phase boundaries of the generalized Pourbaix diagram constructed using the scaling relations obtained from the BEEF-vdW optimal functional. By propagating the uncertainty in the scaling relations, we quantify the confidence in the predictions as shown in the color map. Regions of the plot with low c value are correlated with the positions of surface phase boundaries, similar to that observed for the Pourbaix diagrams on individual rutile oxides.

resolution of material candidates, which implies a larger distinguishability of materials[24] on the descriptor scale as can be seen on the basis of the slopes (<1) of scaling relations defined relative to the chosen material descriptor in Figure 2. An alternate approach could be to choose the descriptor that maximizes prediction efficiency as shown in our earlier work.[24] For this work, we proceed with the choice of O^c as the descriptor in order to perform comparison with the results of Hansen et al.[5] In this representation, we fix the pH and Cl^- concentration (pH 0, $a_{Cl^-} = 1$), but their effects can be easily incorporated by changing the free energies of the various intermediate species accordingly. The species predicted in the generalized surface phase diagram as shown in Figure 3 are consistent with those predicted by Hansen et al.,[5] although the positions of phase boundaries differ slightly. It is worth noting that, in the weaker binding limit, i.e., $\Delta E_{O^c} > 3.6$ eV (determined using the best-fit functional scaling relations), oxygen association at the cus site becomes exothermic, leading to the reaction $O_2^{cc} \rightarrow O_2(g) + 2\,c$ becoming spontaneous. Therefore, the formation of the phases ClO^c and $Cl(O^c)_2$ is unfavorable on catalyst materials with $\Delta E_{O^c} > 3.6$ eV, and we only consider OH^c, Cl^c, and the clean surface as the possible stable surfaces states in this regime.

In the single-descriptor picture, quantifying uncertainty in predictions becomes highly crucial, since the uncertainty in DFT calculations is coupled with that in the scaling relations. We incorporate the uncertainty in scaling relations to quantify the confidence in predicted stable surface species. We generate an ensemble of predicted adsorption energies using the BEEF-vdW functional, which results in an ensemble of scaling relations for each adsorbate. Therefore, for each of the generated GGA-level XC, we can create a unique generalized Pourbaix diagram. We calculate the c value of our predictions by finding the fraction of the functionals in agreement with the hypothesis corresponding to the BEEF-vdW best-fit functional at given values of U and ΔE_{O^c} as described in section 2.2. We find that the c value (Figure 3) of the predictions at the phase boundaries is the lowest, suggesting that a precise determination of stable molecular states at these phase boundaries is computationally challenging. Lower c values at phase boundaries originate from the uncertainty in scaling relationship(s) that are required to describe the phase boundary location. For instance, the phase boundary between the stable surface states O^c and ClO^c determined by $\Delta G(ClO^c) - \Delta G(O^c) - eU = 0$ requires the scaling relation between $\Delta G(ClO^c)$ and $\Delta G(O^c)$ to be expressed in terms of the chosen material descriptor. Similarly, the relatively higher uncertainty observed at the phase boundary between the stable surfaces states ClO^c and $(O^c)_2Cl$ can be explained on the basis of the fact that it requires propagation of uncertainty from two scaling relations involving $\Delta G(O^c)$. Section 7 of the Supporting Information provides a metric to quantify the likelihood of a certain surface state being the most stable by taking into account all of the members of the ensemble of functionals. It is worth pointing out that, in this quantifying propagation formalism, although the discrepancy error of the scaling relations is not explicitly accounted for in this work, it is expected that the considered ensemble of scaling relations corresponding to the ensemble of functionals partially represents the distribution that would arise from a linear least-squares minimization for the fit with a tolerance.

For reducing uncertainty in predictions, surface phase diagrams with U and pH need to be constructed for each

DOI: 10.1021/acscatal.8b01432
ACS Catal. 2018, 8, 9034−9042

given value of ΔE_{O^c} with the associated c values. However, the identification of reaction mechanism trends is not possible with this approach. The generalized Pourbaix diagram with associated c values constructed using the outlined approach maximizes identifiability of trends while retaining the ability to quantify uncertainty in the predictions.

Our analysis suggests the general trend that as the O^c binding strength on materials decreases ($0 < \Delta E_{O^c} < 5$ eV), the stable surface state transitions from being completely covered with O^c to a clean surface. Within this range, we limit our discussions to the chlorine-containing species relevant for identifying the dominant reaction mechanisms. For stronger binding materials, we observe that the Cl^- anion is energetically more favorable as an adsorbed species on O^c (as ClO^c) than on the cation of the clean surface. On relatively more weakly binding materials, we find that the Cl^- anion binds the surface as $(O^c)_2Cl$, which can be explained on the basis of the stability of $(O^c)_2$ relative to $2O^c$. For materials with weak binding ($\Delta E_{O^c} > 3.6$ eV), oxygen can no longer adsorb on the cus site and Cl^- directly adsorbs as Cl^c on the catalyst.

3.3. Limiting Potential and Expected Activity Predictions. Computational screening for active materials requires the understanding of trends in catalytic activity as a function of the chosen material descriptor. For a given material, the activity is governed by the operative reaction mechanism, which is dictated by the stable intermediate species on the surface given by the generalized surface Pourbaix diagram (Figure 3). Invoking linear scaling relationships between the adsorption free energy of oxygen and the adsorption free energies of all the other intermediates allows us to represent both the limiting potential for each mechanism and the stable phase space (generalized Pourbaix diagram) as a function of the same variables—U and ΔE_{O^c} (Figure 4). Overlaying the generalized surface phase diagram with the activity volcano is crucial to obtain the generalized activity volcano (Figure 4) by accounting for the appropriate active reaction mechanism and active site. This results in the activity being governed by reaction mechanism I for strong-binding materials ($\Delta E_{O^c} < \lesssim 2.1$ eV), by reaction mechanism I for moderate-binding materials ($2.1 \lesssim \Delta E_{O^c} \lesssim 3.6$ eV), and by reaction mechanism III for weak-binding materials ($\Delta E_{O^c} \gtrsim 3.6$ eV).

Such single-descriptor activity-prediction models have been successful in determining promising catalysts for various electrochemical reactions including hydrogen evolution,[34,46,50] oxygen reduction,[45,51] hydrogen peroxide synthesis,[52−54] and oxygen evolution.[27,55] Alongside, we address an associated question of the level of confidence in activity predictions and identify material descriptor regimes where the prediction uncertainty is low. We incorporate the uncertainty in scaling relationships and use a Bayesian error estimation approach using the BEEF-vdW XC to quantify the confidence in the predictions of reaction mechanisms and thereby the activity for chlorine evolution. The XC functional generates an ensemble of adsorption energies, as shown in Figure S1, that results in an ensemble of scaling relations for each of the intermediates. Hence, each GGA-level XC functional generated within the ensemble leads to a unique generalized Pourbaix diagram and an associated generalized activity volcano. At a given ΔE_{O^c}, the specific reaction mechanism active for chlorine evolution which governs the limiting potential can hence be determined by the associated stable intermediate species through the generalized Pourbaix diagram. Therefore, for a given value of the material descriptor, ΔE_{O^c}, we can now find a distribution of the predicted limiting potentials corresponding to the family of functionals. This can be used to construct a probability map of the limiting potential for a range of descriptor values, as can be seen in Figure 4. We report $U_{EL}(\Delta E_{O^c})$, the expectation value of the limiting potential, which is computed as the probability-weighted average (refer to section 2.3) of the $U_L(\Delta E_{O^c})$ value.[23,24]

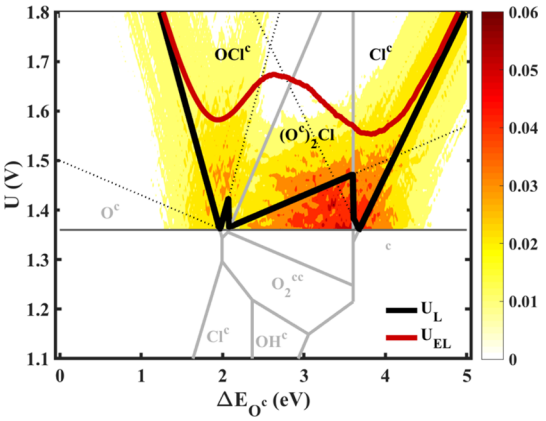

Figure 4. Black dotted lines representing the activity volcano relationships for the possible reaction pathways involving ClO^c, $Cl(O^c)_2$, and Cl^c (left to right) as a function of ΔE_{O^c}, predicted on the basis of the best-fit functional overlaid on the generalized Pourbaix diagram. The stable surface phases are labeled in gray, and the gray lines indicate surface phase boundaries. The bold black lines show the generalized limiting potential relationship (U_L) as a function of ΔE_{O^c} and are constructed by taking into account the stability of the underlying reaction intermediates using the BEEF-vdW optimal functional scaling relations. The color map represents the dimensionless probability distribution of the limiting potential quantified using the ensemble of functionals within the BEEF-vdW XC functional.[24] The red line shows $U_{EL}(\Delta E_{O^c})$, the expectation value of the limiting potentials which is computed as the probability-weighted average of the U_L distribution at each descriptor value. We observe a large deviation of U_{EL} from the U_L for $2.1 \lesssim \Delta E_{O^c} \lesssim 3.6$ eV, where the reaction mechanism mediated by $(O^c)_2Cl$ is predicted to be active for chlorine evolution. We attribute this difference to the fact that the construction of the activity volcano for this reaction pathway involves two scaling relations, which increase the uncertainty in the predictions.

We observe that the U_{EL} curve overlaps with the U_L curve away from the peaks of the volcanoes owing to low prediction uncertainty. Similar observations have been made for hydrogen evolution, oxygen reduction, and oxygen evolution reactions.[24] It is worth pointing out that the U_{EL} predictions based on the activity volcano for the reaction pathway mediated by $Cl(O^c)_2$ and O_2^{cc} are relatively much higher than the U_L values. This can be rationalized partially on the basis of the fact that the activity relationship for this pathway alone involves uncertainty incorporation from two scaling relations: ($\Delta E_{O_2^{cc}}$ and $\Delta E_{Cl(O^c)_2}$ as functions of ΔE_{O^c}). A similar observation was reported for the predicted activity of transition metals for the oxygen reduction reaction using ΔE_O* as the descriptor.[24] Additional factors that lower the prediction confidence in this regime are the low associated c values ($\lesssim 0.55$) for regions in the generalized surface Pourbaix diagram where $Cl(O^c)_2$ and O_2^{cc} are predicted to be the most stable surface state, as can be seen in Figure 3. Hence, DFT predictions of chlorine evolution activity for ΔE_{O^c} approximately in the range 2.1−3.6 eV are subject to higher uncertainty. We argue that $U_{EL}(\Delta E_{O^c})$ is a more relevant activity measure since it explicitly incorporates DFT uncertainty.

DOI: 10.1021/acscatal.8b01432
ACS Catal. 2018, 8, 9034−9042

3.4. Quantifying Confidence in the Predicted Active Reaction Pathway. In reaction schemes involving multiple pathways, an equally important question involves identifying the dominant reaction pathway as a function of the material descriptor. Here, we address the question of propagating the uncertainty associated with adsorption energies and scaling relations to quantify the confidence in predicted reaction pathway. This allows us to predict the active reaction mechanism for chlorine evolution for any new catalyst surface, to a first approximation, through the adsorption free energy of oxygen on the oxide (ΔE_{O^c}) as the descriptor. We determine the confidence in the predicted reaction mechanism through the metric defined in section 2.4, $c_{m_{pred}}$, as a function of ΔE_{O^c}. $c_{m_{pred}}(\Delta E_{O^c})$ is calculated on the basis of the level of agreement between the predicted reaction mechanism(s) by the ensemble of GGA-level functionals and the BEEF-vdW optimal functional. We define another useful quantity, $c_{m_{pred}=i}$ for the ith reaction mechanism, which becomes especially important in regimes where the $c_{m_{pred}}$ value is less than 1, where different functionals identify different reaction mechanisms to be active. $c_{m_{pred}=i}(\Delta E_{O^c})$ provides a measure of the confidence for the ith reaction mechanism being active (refer to eq 4).

On the basis of the definition of $c_{m_{pred}=i}$ we highlight a property of interest: the sum of $c_{m_{pred}=i}$ (i = 1, 2, ..., n_{mech}) for any given value of the descriptor ΔE_{O^c} is equal to 1. This implies that the confidence values corresponding to all mechanisms cannot simultaneously increase or decrease in any ΔE_{O^c} range. The rule can be expressed as

$$\sum_{i=1}^{n_{mech}} c_{m_{pred}=i}(\Delta E_{O^c}) = \sum_{i=1}^{n_{mech}} \left[\frac{1}{N_{ens}} \sum_{n=1}^{N_{ens}} \delta(m^n_{pred}(\Delta E_{O^c}) - i) \right] = 1$$

We observe (Figure 5) that for materials with strong oxygen binding ($0 \lesssim \Delta E_{O^c} \lesssim 2.1$ eV), the majority of functionals predict that chlorine evolution occurs by the reaction mechanism mediated by ClO^c ($c_{m_{pred}} \approx c_{m_{pred}=1} \approx 1$). In the range of materials that moderately bind oxygen on the cus cite ($2.1 \lesssim \Delta E_{O^c} \lesssim 3.6$ eV), we observe that there exists a lower degree of agreement between the functionals with respect to the predicted reaction mechanisms, leading to relatively low $c_{m_{pred}}$ values, although most functionals are in agreement with the optimal around $\Delta E_{O^c} \approx 3$ eV. For materials that bind oxygen weakly on the cus site (ΔE_{O^c} > 3.6 eV), it is thermodynamically favorable to have the chlorine intermediate directly adsorbed on the cus site (as Cl^c) rather than on oxygen (as either ClO^c or $(O_2^c)Cl$). In this regime, we find that the majority of functionals agree with the BEEF-vdW optimal functional, and chlorine evolution is mediated with a high certainty by the reaction pathway mediated by Cl^c. We show that materials RuO_2 and IrO_2 that form dimensionally stable anodes (DSA) proceed through the ClO^c-mediated pathway with high certainty (c value = 1). TiO_2 proceeds through the pathway mediated by Cl^c with high certainty (c value = 0.94), while PtO_2 proceeds through the pathway mediated by $Cl(O^c)_2$ with a c value of 0.61.

It is worth noting that different functionals may identify the same reaction pathway as the dominant one. However, they may result in vastly different limiting potentials. This raises an important question on the confidence associated with identifying reaction mechanisms versus determining activity values. This can be analyzed through an example case of RuO_2, where ΔE_{O^c} = 1.53 eV. In this case, all the functionals identify the ClO^c-mediated pathway to be the active one. However, the functionals identify vastly different limiting potentials, as shown in Figure S7. This leads to an important conclusion that the confidence in utilizing DFT calculations for the classification problem of identifying the dominant reaction mechanism is much better than the prediction problem of determining the catalytic activity. This has an important implication more broadly that DFT-identified reaction pathways are likely to be much more robust than the DFT-predicted catalytic activities.

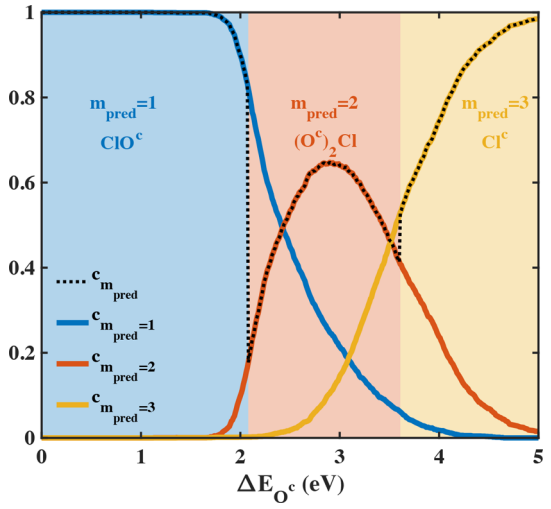

Figure 5. Quantifying the confidence in the predicted reaction mechanism $c_{m_{pred}}$ as a function of the material descriptor (black dotted line). The bold lines represent the confidence in the reaction mechanisms mediated by the stable intermediates ClO^c ($c_{m_{pred}=1}$), $(O^c)_2Cl$ ($c_{m_{pred}=2}$), and Cl^c ($c_{m_{pred}=3}$). The colored regions in the plot represent the reaction mechanism predicted by the BEEF-vdW (best-fit) optimal functional. We observe relatively low $c_{m_{pred}}$ values for the reaction mechanism mediated by intermediate $(O^c)_2Cl$ in the material descriptor range $2.1 \lesssim \Delta E_{O^c} \lesssim 3.6$ eV, implying a higher degree of disagreement between the GGA-level functionals within the ensemble of functionals.

4. CONCLUSIONS

We demonstrate an approach to quantify the confidence associated with predictions of the activity-governing reaction mechanism by systematically accounting for the uncertainty derived from the DFT-calculated adsorption energetics. By using the c value in the context of Pourbaix diagrams as a metric to quantify the level of confidence in surface state predictions, we highlight and rationalize the origin of higher uncertainty close to phase boundaries. We quantitatively suggest with high confidence that chlorine evolution on RuO_2 and IrO_2 occurs through the reaction mechanism mediated by ClO^c. To analyze trends in the predicted stable surface states across materials, we construct a generalized Pourbaix diagram by invoking scaling relations between the surface intermediate species. We choose ΔE_{O^c} as the material descriptor, since it allows greater resolution of material candidates on the descriptor scale. By overlaying the generalized surface phase diagram with the activity relationships, we construct the generalized activity volcano by accounting for the appropriate operative reaction mechanism. Incorporating the uncertainty in the scaling relations, we report the prediction confidence in the generalized Pourbaix diagram and find the

DOI: 10.1021/acscatal.8b01432
ACS Catal. 2018, 8, 9034−9042

distribution of the limiting potential as a function of the material descriptor. We compute the expected activity, $U_{EL}(\Delta E_{O^c})$, which we argue is a more relevant activity measure since it incorporates DFT uncertainty. Furthermore, we quantify the robustness of the prediction of the likely operative reaction mechanism as a function of the chosen material descriptor, which we believe is crucial for improving the accuracy of activity predictions in descriptor-based catalyst screening approaches. It is worth highlighting that while this work focuses on the robustness of predictions based on the uncertainty within GGA-level functionals, an important secondary question that remains to be answered is the influence of higher-order functionals on the confidence of predictions. Finally, we find that materials which form dimensionally stable anodes (DSA), RuO_2 and IrO_2, proceed through the ClO^c-mediated pathway with very high confidence (c value = 1). TiO_2 proceeds through the Cl^c-mediated pathway with high confidence (c value = 0.94), while PtO_2 proceeds through the $Cl(O^c)_2$-mediated pathway with a c value of 0.61. Although this work focuses on the mechanisms by which chlorine evolution can occur, the presented approach can readily be extended not only to other multielectron reactions involving multiple reaction pathways but also to reactions where the selectivity of products is critical.

■ ASSOCIATED CONTENT

Supporting Information

The Supporting Information is available free of charge on the ACS Publications website at DOI: 10.1021/acscatal.8b01432.

Computational details, adsorption energetics of all the considered surface states, scaling relationships, Pourbaix diagram construction, and uncertainty propagation framework for chlorine evolution activity (PDF)

■ AUTHOR INFORMATION

Corresponding Author

*E-mail for V.V.: venkvis@cmu.edu.

ORCID

Vaidish Sumaria: 0000-0002-0263-749X

Dilip Krishnamurthy: 0000-0001-8231-5492

Venkatasubramanian Viswanathan: 0000-0003-1060-5495

Notes

The authors declare no competing financial interest.

■ ACKNOWLEDGMENTS

The authors thank Dr. Heine A. Hansen for insightful discussions and for sharing structure files. D.K. and V.V. gratefully acknowledge funding support from the National Science Foundation under award CBET-1554273. V.S. and V.V. acknowledge support from the Scott Institute for Energy Innovation at Carnegie Mellon University.

■ REFERENCES

(1) Bockris, J. O. J. O.; Khan, S. U. M. *Surface Electrochemistry: A Molecular Level Approach*; Plenum: New York, 1993; pp 211−405.

(2) Hansen, H. A.; Rossmeisl, J.; Nørskov, J. K. Surface Pourbaix Diagrams and Oxygen Reduction Activity of Pt, Ag and Ni(111) Surfaces Studied by DFT. *Phys. Chem. Chem. Phys.* **2008**, *10*, 3722−3730.

(3) Yan, B.; Krishnamurthy, D.; Hendon, C. H.; Deshpande, S.; Surendranath, Y.; Viswanathan, V. Surface Restructuring of Nickel Sulfide Generates Optimally Coordinated Active Sites for Oxygen Reduction Catalysis. *Joule* **2017**, *1*, 600−612.

(4) Bajdich, M.; García-Mota, M.; Vojvodic, A.; Nørskov, J. K.; Bell, A. T. Theoretical Investigation of the Activity of Cobalt Oxides for the Electrochemical Oxidation of Water. *J. Am. Chem. Soc.* **2013**, *135*, 13521−13530.

(5) Hansen, H. A.; Man, I. C.; Studt, F.; Abild-Pedersen, F.; Bligaard, T.; Rossmeisl, J. Electrochemical Chlorine Evolution at Rutile Oxide (110) Surfaces. *Phys. Chem. Chem. Phys.* **2010**, *12*, 283−290.

(6) Skúlason, E.; Karlberg, G. S.; Rossmeisl, J.; Bligaard, T.; Greeley, J.; Jónsson, H.; Nørskov, J. K. Density Functional Theory Calculations for the Hydrogen Evolution Reaction in an Electrochemical Double Layer on the Pt(111) Electrode. *Phys. Chem. Chem. Phys.* **2007**, *9*, 3241−3250.

(7) Montoya, J. H.; Tsai, C.; Vojvodic, A.; Nørskov, J. K. The Challenge of Electrochemical Ammonia Synthesis: A New Perspective on The Role of Nitrogen Scaling Relations. *ChemSusChem* **2015**, *8*, 2180−2186.

(8) Kuhl, K. P.; Cave, E. R.; Abram, D. N.; Jaramillo, T. F. New Insights into the Electrochemical Reduction of Carbon Dioxide on Metallic Copper Surfaces. *Energy Environ. Sci.* **2012**, *5*, 7050−7059.

(9) Hori, Y.; Murata, A.; Takahashi, R. Formation of Hydrocarbons in The Electrochemical Reduction of Carbon Dioxide at a Copper Electrode in Aqueous Solution. *J. Chem. Soc., Faraday Trans. 1* **1989**, *85*, 2309−2326.

(10) Hori, Y.; Takahashi, R.; Yoshinami, Y.; Murata, A. Electrochemical Reduction of CO on a Copper Electrode. *J. Phys. Chem. B* **1997**, *101*, 7075−7081.

(11) Schouten, K.; Kwon, Y.; Van der Ham, C.; Qin, Z.; Koper, M. A New Mechanism for the Selectivity to C 1 And C 2 Species in the Electrochemical Reduction of Carbon Dioxide on Copper Electrodes. *Chem. Sci.* **2011**, *2*, 1902−1909.

(12) DeWulf, D. W.; Jin, T.; Bard, A. J. Electrochemical and Surface Studies of Carbon Dioxide Reduction to Methane and Ethylene at Copper Electrodes in Aqueous Solutions. *J. Electrochem. Soc.* **1989**, *136*, 1686−1691.

(13) Peterson, A. A.; Abild-Pedersen, F.; Studt, F.; Rossmeisl, J.; Nørskov, J. K. How Copper Catalyzes the Electroreduction of Carbon Dioxide into Hydrocarbon Fuels. *Energy Environ. Sci.* **2010**, *3*, 1311−1315.

(14) Schouten, K. J. P.; Qin, Z.; Pérez Gallent, E.; Koper, M. T. Two Pathways for the Formation of Ethylene in Co Reduction on Single-Crystal Copper Electrodes. *J. Am. Chem. Soc.* **2012**, *134*, 9864−9867.

(15) Krishtalik, L. Kinetics and Mechanism of Anodic Chlorine and Oxygen Evolution Reactions on Transition Metal Oxide Electrodes. *Electrochim. Acta* **1981**, *26*, 329−337.

(16) Wieckowski, A.; Neurock, M. Contrast and Synergy Between Electrocatalysis and Heterogeneous Catalysis. *Adv. Phys. Chem.* **2011**, *2011*, 1−18.

(17) Mukerjee, S.; Srinivasan, S.; Soriaga, M. P.; McBreen, J. Role of Structural and Electronic Properties of Pt And Pt Alloys on Electrocatalysis of Oxygen Reduction an in Situ XANES and EXAFS Investigation. *J. Electrochem. Soc.* **1995**, *142*, 1409−1422.

(18) Iwasita, T. *Infrared Spectroscopy in Electrochemistry*; Elsevier Science: 1996; Vol. *41*, pp 621−781.

(19) Wakisaka, M.; Suzuki, H.; Mitsui, S.; Uchida, H.; Watanabe, M. Identification and Quantification of Oxygen Species Adsorbed on Pt (111) Single-Crystal and Polycrystalline Pt Electrodes by Photoelectron Spectroscopy. *Langmuir* **2009**, *25*, 1897−1900.

(20) Su, H.-Y.; Gorlin, Y.; Man, I. C.; Calle-Vallejo, F.; Nørskov, J. K.; Jaramillo, T. F.; Rossmeisl, J. Identifying Active Surface Phases for Metal Oxide Electrocatalysts: A Study of Manganese Oxide Bi-Functional Catalysts for Oxygen Reduction and Water Oxidation Catalysis. *Phys. Chem. Chem. Phys.* **2012**, *14*, 14010−14022.

(21) Mortensen, J. J.; Kaasbjerg, K.; Frederiksen, S. L.; Nørskov, J. K.; Sethna, J. P.; Jacobsen, K. W. Bayesian Error Estimation in Density-Functional Theory. *Phys. Rev. Lett.* **2005**, *95*, 216401.

(22) Medford, A. J.; Wellendorff, J.; Vojvodic, A.; Studt, F.; Abild-Pedersen, F.; Jacobsen, K. W.; Bligaard, T.; Nørskov, J. K. Assessing the Reliability of Calculated Catalytic Ammonia Synthesis Rates. *Science* **2014**, *345*, 197−200.

DOI: 10.1021/acscatal.8b01432
ACS Catal. 2018, 8, 9034−9042

(23) Deshpande, S.; Kitchin, J. R.; Viswanathan, V. Quantifying Uncertainty in Activity Volcano Relationships for Oxygen Reduction Reaction. *ACS Catal.* **2016**, *6*, 5251−5259.
(24) Krishnamurthy, D.; Sumaria, V.; Viswanathan, V. Maximal Predictability Approach for Identifying the Right Descriptors for Electrocatalytic Reactions. *J. Phys. Chem. Lett.* **2018**, *9*, 588−595.
(25) O'Brien, T. F.; Bommaraju, T. V.; Hine, F. *Handbook of Chlor-Alkali Technology*; Springer US: 2005; pp 37−74.
(26) Trasatti, S. Electrocatalysis in the Anodic Evolution of Oxygen and Chlorine. *Electrochim. Acta* **1984**, *29*, 1503−1512.
(27) Man, I. C.; Su, H.-Y.; Calle-Vallejo, F.; Hansen, H. A.; Martínez, J. I.; Inoglu, N. G.; Kitchin, J.; Jaramillo, T. F.; Nørskov, J. K.; Rossmeisl, J. Universality in Oxygen Evolution Electrocatalysis on Oxide Surfaces. *ChemCatChem* **2011**, *3*, 1159−1165.
(28) Viswanathan, V.; Hansen, H. A. Unifying Solution and Surface Electrochemistry: Limitations and Opportunities in Surface Electrocatalysis. *Top. Catal.* **2014**, *57*, 215−221.
(29) Mortensen, J. J.; Hansen, L. B.; Jacobsen, K. W. Real-Space Grid Implementation of the Projector Augmented Wave Method. *Phys. Rev. B: Condens. Matter Mater. Phys.* **2005**, *71*, 035109.
(30) Enkovaara, J. E.; Rostgaard, C.; Mortensen, J. J.; Chen, J.; Dułak, M.; Ferrighi, L.; Gavnholt, J.; Glinsvad, C.; Haikola, V.; Hansen, H. Electronic Structure Calculations with GPAW: A Real-Space Implementation of the Projector Augmented-Wave Method. *J. Phys.: Condens. Matter* **2010**, *22*, 253202.
(31) Wellendorff, J.; Lundgaard, K. T.; Møgelhøj, A.; Petzold, V.; Landis, D. D.; Nørskov, J. K.; Bligaard, T.; Jacobsen, K. W. Density Functionals for Surface Science: Exchange-Correlation Model Development with Bayesian Error Estimation. *Phys. Rev. B: Condens. Matter Mater. Phys.* **2012**, *85*, 235149.
(32) Ahmad, Z.; Viswanathan, V. Quantification of Uncertainty in First-Principles Predicted Mechanical Properties of Solids: Application to Solid Ion Conductors. *Phys. Rev. B: Condens. Matter Mater. Phys.* **2016**, *94*, 064105.
(33) Houchins, G.; Viswanathan, V. Quantifying Confidence in Density Functional Theory Predictions of Magnetic Ground States. *Phys. Rev. B: Condens. Matter Mater. Phys.* **2017**, *96*, 134426.
(34) Nørskov, J. K.; Bligaard, T.; Logadottir, A.; Kitchin, J.; Chen, J. G.; Pandelov, S.; Stimming, U. Trends in The Exchange Current for Hydrogen Evolution. *J. Electrochem. Soc.* **2005**, *152*, J23−J26.
(35) Karlberg, G.; Rossmeisl, J.; Nørskov, J. K. Estimations of Electric Field Effects on the Oxygen Reduction Reaction Based on the Density Functional Theory. *Phys. Chem. Chem. Phys.* **2007**, *9*, 5158−5161.
(36) Gauthier, J. A.; Dickens, C. F.; Chen, L. D.; Doyle, A. D.; Norskov, J. K. Solvation Effects for Oxygen Evolution Reaction Catalysis on IrO_2(110). *J. Phys. Chem. C* **2017**, *121*, 11455−11463.
(37) He, Z.-D.; Hanselman, S.; Chen, Y.-X.; Koper, M. T. M.; Calle-Vallejo, F. Importance of Solvation for the Accurate Prediction of Oxygen Reduction Activities of Pt-Based Electrocatalysts. *J. Phys. Chem. Lett.* **2017**, *8*, 2243−2246.
(38) Calle-Vallejo, F.; Krabbe, A.; Garcia-Lastra, J. M. How Covalence Breaks Adsorption-Energy Scaling Relations and Solvation Restores them. *Chem. Sci.* **2017**, *8*, 124−130.
(39) Thiel, P. A.; Madey, T. E. The Interaction of Water With Solid Surfaces: Fundamental Aspects. *Surf. Sci. Rep.* **1987**, *7*, 211−385.
(40) Limmer, D. T.; Willard, A. P.; Madden, P.; Chandler, D. Hydration of Metal Surfaces Can Be Dynamically Heterogeneous and Hydrophobic. *Proc. Natl. Acad. Sci. U. S. A.* **2013**, *110*, 4200−4205.
(41) Henderson, M. A. The Interaction of Water With Solid Surfaces: Fundamental Aspects Revisited. *Surf. Sci. Rep.* **2002**, *46*, 1−308.
(42) Zeng, Z.; Greeley, J. Characterization of Oxygenated Species at Water/Pt (111) Interfaces From DFT Energetics and XPS Simulations. *Nano Energy* **2016**, *29*, 369−377.
(43) Rossmeisl, J.; Qu, Z.-W.; Zhu, H.; Kroes, G.-J.; Nørskov, J. K. Electrolysis of water on oxide surfaces. *J. Electroanal. Chem.* **2007**, *607*, 83−89.
(44) Hansen, H. A.; Viswanathan, V.; Nørskov, J. K. Unifying Kinetic and Thermodynamic Analysis of $2e^-$ and $4e^-$ Reduction of Oxygen on Metal Surfaces. *J. Phys. Chem. C* **2014**, *118*, 6706−6718.
(45) Viswanathan, V.; Hansen, H. A.; Rossmeisl, J.; Nørskov, J. K. Universality in Oxygen Reduction Electrocatalysis on Metal Surfaces. *ACS Catal.* **2012**, *2*, 1654−1660.
(46) Greeley, J.; Nørskov, J. K.; Kibler, L. A.; El-Aziz, A. M.; Kolb, D. M. Hydrogen Evolution Over Bimetallic Systems: Understanding the Trends. *ChemPhysChem* **2006**, *7*, 1032−1035.
(47) Exner, K. S.; Anton, J.; Jacob, T.; Over, H. Controlling Selectivity in the Chlorine Evolution Reaction over RuO2-Based Catalysts. *Angew. Chem., Int. Ed.* **2014**, *53*, 11032−11035.
(48) Wang, H.; Schneider, W. F.; Schmidt, D. Intermediates and Spectators in O_2dissociation at the RuO2 (110) Surface. *J. Phys. Chem. C* **2009**, *113*, 15266−15273.
(49) Pankratiev, Y. D. Correlation Between Oxygen Binding Energy and Catalytic Activity of Oxides. *React. Kinet. Catal. Lett.* **1982**, *20*, 255−259.
(50) Greeley, J.; Jaramillo, T. F.; Bonde, J.; Chorkendorff, I.; Nørskov, J. K. Computational High-Throughput Screening of Electrocatalytic Materials for Hydrogen Evolution. *Nat. Mater.* **2006**, *5*, 909−913.
(51) Greeley, J.; Nørskov, J. K. Combinatorial Density Functional Theory-Based Screening of Surface Alloys for the Oxygen Reduction Reaction. *J. Phys. Chem. C* **2009**, *113*, 4932−4939.
(52) Rankin, R. B.; Greeley, J. Trends In Selective Hydrogen Peroxide Production on Transition Metal Surfaces from First Principles. *ACS Catal.* **2012**, *2*, 2664−2672.
(53) Viswanathan, V.; Hansen, H. A.; Nørskov, J. K. Selective Electrochemical Generation of Hydrogen Peroxide from Water Oxidation. *J. Phys. Chem. Lett.* **2015**, *6*, 4224−4228.
(54) Verdaguer-Casadevall, A.; Deiana, D.; Karamad, M.; Siahrostami, S.; Malacrida, P.; Hansen, T. W.; Rossmeisl, J.; Chorkendorff, I.; Stephens, I. E. Trends in The Electrochemical Synthesis Of H_2O_2: Enhancing Activity and Selectivity by Electrocatalytic Site Engineering. *Nano Lett.* **2014**, *14*, 1603−1608.
(55) Halck, N. B.; Petrykin, V.; Krtil, P.; Rossmeisl, J. Beyond the Volcano Limitations in Electrocatalysis−Oxygen Evolution Reaction. *Phys. Chem. Chem. Phys.* **2014**, *16*, 13682−13688.

DOI: 10.1021/acscatal.8b01432
ACS Catal. 2018, 8, 9034−9042